Journal of Environmental Chemical Engineering 12 (2024) 112911

Contents lists available at ScienceDirect

Journal of Environmental Chemical Engineering

journal homepage: www.elsevier.com/locate/jece

Exploring the adsorption of five emerging pollutants on activated carbon: A theoretical approach

Lisdelys González-Rodríguez [a,b], Osvaldo Yáñez [b], Karel Mena- Ulecia [c,d], Yoan Hidalgo-Rosa [e,f], Ximena García- Carmona [g], Claudia Ulloa- Tesser [h,*]

[a] Facultad de Ingeniería y Negocios, Universidad de Las Américas, Sede Concepción, Concepción 4030000, Chile
[b] Núcleo de Investigación en Data Science (NIDS), Facultad de Ingeniería y Negocios, Universidad de Las Américas, Santiago 7500000, Chile
[c] Universidad Católica de Temuco, Facultad de Recursos Naturales, Departamento de Ciencias Biológicas y Químicas, Temuco 4780000, Chile
[d] Núcleo de Investigación en Bioproductos y Materiales Avanzados (BIOMA), Facultad de Ingeniería, Universidad Católica de Temuco, Temuco 4780000, Chile
[e] Departamento de Química Inorgánica, Facultad de Química y de Farmacia, Pontificia Universidad Católica de Chile, Vicuña Mackenna 4860, Santiago 7500000, Chile
[f] Facultad de Ingeniería, Universidad Finis Terrae, Av. Pedro de Valdivia 1509, Santiago 7500000, Chile
[g] Carbon and Catalysis Laboratory (CarboCat), Department of Chemical Engineering, Universidad de Concepción, Concepción 4030000, Chile
[h] Environmental Engineering Department, Faculty of Environmental Sciences and EULA Chile Centre, Universidad de Concepción, Concepción 4030000, Chile

ARTICLE INFO

Keywords:
Activated carbon
Contaminants of emerging concern
DFT studies

ABSTRACT

The identification and management of contaminants of emerging concern (CECs) in water systems is crucial for protecting public and environmental health. This paper reports a theoretical approach to studying the adsorption of five CECs: Atrazine (ATZ), Caffeine (CAF), Carbamazepine (CBZ), Sulfamethoxazole (SMX), and Ibuprofen (IBU) - onto Activated Carbon (AC). A set of computational methods, including electrostatic molecular potential maps, conceptual density functional theory, Fukui functions, thermodynamic analysis, and tight-binding molecular dynamics simulations, were employed to analyze the electronic/energetic interactions and mechanisms involved in the adsorption of CECs on AC. The theoretical methodology offered valuable predictions on reactivity sites, stability, and binding mechanisms. Results showed that adsorption primarily occurred through non-covalent interactions like π-π electron donor-acceptor interactions, van der Waals forces, and hydrophobic interactions. Thermodynamic properties suggested the adsorption process was spontaneous and exothermic. However, for the AC/SMX system, the Gibbs free energy reveals that adsorption may be unfavorably compared to the other study systems. Molecular dynamics simulations validated the kinetic stability in the following order CAF (0.13 Å)>CBZ (0.23 Å)>ATZ (0.75 Å)> IBU (1.28 Å)>SMX (1.54 Å). This exploratory theoretical study provides a deep understanding of the interactions between AC and five CECs, aiding in the rational design and optimization of AC-based treatment systems for environmental and industrial applications.

1. Introduction

In recent years, a group of anthropogenic substances present in the urban water cycle has begun to cause concerns about their potential effects on human health and aquatic ecosystems. These are the so-called contaminants of emerging concern (CECs), which, include pharmaceuticals, personal care products, microplastics, viruses, resistance genes, toxic disinfection products, as well as all organic chemicals [1], which enter urban water systems mainly through discharges from sewage treatment plants. A significant part of those substances is not treated nor destroyed in water treatment plants, and they are spread in the environment[2]. These substances exert adverse effects on human health, including neurotoxicity, reproductive toxicity, metabolic interference, and antibiotic resistance [3]. Among these CECs, are herbicides, stimulants, antibiotics, anticonvulsants, and nonsteroidal anti-inflammatory drugs (NSAIDs). Caffeine (CAF) is a known stimulant that significantly contributes to water pollution and is frequently used as an indicator of anthropogenic water pollution[4]. Sulfamethoxazole (SMX) is an antibiotic, widely used in human and veterinary medication to prevent and treat diseases and is one of the most frequently detected antibiotics in surface water and wastewater [5]. Carbamazepine (CBZ) is a pharmaceutical used as an anticonvulsant drug and is reported as one of the recurrently detected CECs in water bodies [6]. Among the available NSAIDs, ibuprofen (IBU) is one of the most consumed worldwide, after

* Corresponding author.
E-mail address: claudiaulloa@udec.cl (C. Ulloa- Tesser).

https://doi.org/10.1016/j.jece.2024.112911
Received 1 February 2024; Received in revised form 23 April 2024; Accepted 26 April 2024
Available online 29 April 2024

ingestion by humans and animals, IBU is not completely metabolized and is released into sewage treatment plants [7]. Atrazine (ATZ) is an herbicide used to control broadleaf weeds and grasses in agriculture. Its intensive use added to a low biodegradability, high mobility in the environment, long half-life and high leaching capacity explains the presence of ATZ in ground and surface water [8].

For the removal of CECs, chemical advanced treatments, such as advanced oxidative processes [9] and physical treatments (e.g. ultrafiltration membranes) can be used [10]. Adsorption is a promising treatment because it features a simple design, easy operation, and low initial cost[11]. Compared to other technologies, it has the advantage that no intermediates are produced during the process, which can be more toxic than the parent compound [12]. Several experimental studies have been conducted to investigate the removal of CAF [13,14], SMX [15,16], CBZ [17–19], IBU [20,21]and ATZ [22,23] from water by applying activated carbon (AC). The adsorption capacity of an AC depends on its physicochemical characteristics (surface area, pore size, functional groups, point of zero charge) and the nature of the adsorbate (molecular weight and size, hydrophobicity, polarity) [24]. On the other hand, owing to the heterogeneous nature of AC, arising from differing feedstock compositions and activation conditions, the effectiveness of AC displays variability.

Also, experimental adsorption studies contain several steps, such as knowing the effect of pH and ionic strength, kinetics, isotherms, thermodynamics, desorption, and regeneration, making them very intensive in terms of time, energy, and material requirements [25]. In this sense, theoretical studies are a tool to make the best use of limited resources and to explore a wide range of experimental scenarios gaining a better understanding of the mechanisms involved in the adsorption process of CECs. Density functional theory (DFT) calculations have been proven to be useful tools in the description of the electronic structure of several organic compounds and their response in a molecular system [26–28]. A great number of papers report theoretical research on the structure of AC and the process of their interaction with several organic pollutants [29–32]. In particular, the Fukui function [16–18] offers information about the most reactive sites of the CECs for their interaction with the AC surface, thereby described as local reactivity. The Kick-Fukui method is a hybrid approach to exploring the potential energy surface (PES) of molecules and clusters. It combines the Coulomb integral [33] and Fukui functions to efficiently predict the global minimum of various AC/CECs systems. Another computational method commonly employed to understand various types of non-covalent interactions (NCI), such as dispersive (Van der Waals forces), hydrogen bonds, dipole-dipole interactions, and steric effects [34] Recently, one of us has demonstrated that NCI is a valuable tool for understanding aspects such as chemical bonding, intermolecular forces, molecular packing, etc [35]. Thereby facilitating a quantitative understanding of the weak interactions that influence the structure, function, and properties of molecules. In addition, Ref. [36] has explored the conformational space of molecular systems with tight-binding molecular dynamics simulations, reporting higher accuracy when compared to other semi empirical methods. In general, the CECs and AC are typically regarded as separate entities which has caused a failure to utilize the full benefits offered by computational methods and theoretical chemistry tools for the study of the adsorption process. Therefore, the use of theoretical chemistry tools for the calculation of the several descriptors to study different AC/CECs systems is an alternative to optimize the time, cost, and effort required in the research that is being carried out in our laboratory on the adsorption of CECs on materials such as AC.

The main objective of this study was to develop a theoretical procedure through a computational quantum chemistry approach for deep insights into the nature of interactions between AC and five CECs: Atrazine (ATZ), Caffeine (CAF), Carbamazepine (CBZ), Sulfamethoxazole (SMX), and Ibuprofen (IBU). According to the results, we consider that the theoretical protocol presented here can guide design and experimental research predicting the adsorption mechanism in material like AC for removing CECs. This theoretical study contributes significantly to the understanding of AC capabilities as an adsorbent for CECs and helps researchers design more effective treatment adsorption processes or new material designs.

2. Methodology

All CECs molecules were evaluated for their protonation state at pH = 7.0 *minus*0.2 sed on the experimental data carried out, using the pKa plugin [37,38]. The pKa plugin is a tool provided by ChemAxon that calculates the pKa values of all proton-gaining or losing atoms in a molecule based on the microspecies distribution curves by pH. pKa values are important in understanding the acidity and basicity of molecules, as they indicate the relative ability of a molecule to give up a proton. A low pKa value indicates that the compound is acidic and will easily give up its proton to a base. The pKa plugin calculates pKa values based on the partial charge distribution of the molecule.

In quantum chemical calculations, it is commonly found that a carbon-based material like AC is typically depicted as a single graphene layer. The unsaturated edges of this layer can serve as active sites for adsorption, as the carbon atoms at these edges possess unpaired electrons that are easily transferable. As a result, a zigzag-shaped graphene model containing 54 carbon atoms, along with corresponding functionalized graphite models, is used as the fundamental structure [39,40]. By utilizing this procedure, it becomes possible to model only a fraction of the material, while applying a high level of theory with a molecular modeling program.

Full geometry optimizations, as well as vibrational frequency (absence of imaginary frequencies) of the ATZ, CAF, CBZ, IBU, SMX, and AC molecules, were implemented via DFT with Minnesota hybrid *meta*-GGA functional M06–2X-D3[41,42] and the 6–311++G(d,p) basis set [43], with solvation model based on density (SMD) for the implicit water. SMD is a universal solvation model, where "universal" denotes its applicability to any charged or uncharged solute in any solvent or liquid medium. All global and local chemical reactivity calculations were performed with TAFF software [44,45].

The PES of ATZ, CAF, CBZ, IBU, and SMX on the surface of AC, was explored with the Kick-Fukui algorithm[45–47]. In the Kick-Fukui method, an initial population of 100,000 individuals is preselected using the Fukui function (FF) [48–51]. The FF is used to identify relevant positions on the PES. The structure generation method (Kick) already has certain restrictions that allow for good candidates from the beginning, such as the size of the box and the connectivity analysis between structures. The Kick-Fukui method considers one term of the interaction energy equation (which contains local reactivity information between two interacting species) as the energy interaction descriptor. This allows for the efficient screening of the best individuals. Overall, the Kick-Fukui method is a novel approach to exploring the PES of molecules and clusters that combines the Coulomb integral and Fukui functions to efficiently predict the global minimum of various systems. In this case, the M06–2X-D3/SDDAll [52–55] level was used for the exploration of a total of 10 species, each of which was geometrically optimized at that level. Subsequently, a re-optimization of geometry and calculation of frequencies for the best structure (putative global minima), was performed using the M06–2X functional in conjunction with the 6–31 G (d, p) basis set and the Grimme dispersion correction (D3) in the Gaussian16 package [56]. M06–2X is the best dispersion-corrected meta-GGA hybrid functional on the GMTKN30 database [57]. Water was simulated as a solvent using the SMD parametrization of the IEF-PCM.

To calculate the thermodynamic properties and binding energies we employed specific parameters, namely binding energy (ΔE at 0 K), enthalpy (ΔH), Gibbs free energy (ΔG), and entropy (ΔS) at 298.15 K. These calculations were conducted on the global minima obtained during the exploration of the PES using the supermolecule approximation (refer to Eq. 1). In Eq. 1, the variable *X* represents E, H, G, or S. To

calculate ΔE, we considered the contributions of zero-point energy (ZPE) and basis set superposition error (BSSE) counterpoise corrections. The BSSE corrections helped estimate the basis set superposition error by comparing the properties of the AC/CECs systems with those of individual monomers. We treated AC and pollutants as separate monomers, resulting in a total of 6 monomers: AC, ATZ, CAF, CBZ, IBU, and SMX. Optimization of the properties for both monomers and AC/CECs complex systems was performed, and frequency calculations were conducted using DFT with the hybrid functional M06–2X and a 6–31 G (d,p) basis set. Additionally, Grimme dispersion correction (D3) was applied using the Gaussian 16 software package.

$$\Delta X = X_{system} - (\sum X_{monomer}) \quad (1)$$

The optimized geometry of the AC/CECs systems in their ground (S_0) states was used as input data to perform the intermolecular interactions analysis. In the first step, the Morokuma-Ziegler scheme's energy decomposition analysis (EDA) was used to examine the host-guest interactions [58,59]. The Amsterdam Density Functional (ADF) package was used to conduct this analysis [60] Two components in each AC/CECs system were split, i.e., one fragment standing the AC and the other the corresponding pollutant, namely ATZ, CAF, CBZ, IBU, and SMX. Eq. 2 shows the breakdown of the interaction energy (ΔE_{int}) between the two fragments into four terms.

$$\Delta E_{int} = \Delta E_{Pauli} + \Delta E_{Elec} + \Delta E_{Orb} + \Delta E_{Disp} \quad (2)$$

Where ΔE_{Pauli} term describes the repulsive interaction of Pauli between the occupied orbitals of the two molecular fragments in this instance. The classical electrostatic interaction between the two fragments is denoted by the second term, ΔE_{Elec}. The possible interactions between molecular orbitals (MOs) related to charge transfer, polarization, etc. are considered by the third term, ΔE_{Orb}. The natural orbital chemical valence (NOCV) method, put forth by Mitoraj, can be used to analyze in detail this term [61] The Grimme's D3 dispersion correction for EDA calculations included the term ΔE_{Disp} which refers to the forces of dispersion acting between the fragments[62] Finally, the basis set superposition error (BSSE) counterpoise method was used to correct the interaction energies between AC and pollutants for all systems [63].

The non-covalent interaction index (NCI)[34,64] was used to qualitatively identify the areas where weak interactions predominate in the AC/CECs systems, the origin of which may be dispersive, hydrogen bonds, dipole-dipole interactions, or repulsive steric effects. These are based on the electron density (ρ), its derivatives the reduced density gradient (s), and the sign of the second eigenvalue (λ_2) of the electron density matrix (Hessian matrix). Additionally, we performed the Independent Gradient Model based on the Hirshfeld partition (IGMH) [65]. IGMH is a new method proposed for visually analyzing intramolecular and intermolecular interactions in chemical systems. It builds upon the existing Independent Gradient Model method by replacing the free-state atomic densities used in IGM with atomic densities obtained from Hirshfeld partitioning of the molecular density. This gives IGMH a more rigorous physical basis. IGMH has advantages over other popular visualization methods like Non-covalent Interaction plots. It can separately visualize intrafragment and interfragment interactions with smoother and less jagged isosurfaces. To understand the formation of the AC/CECs systems the Atoms in Molecules (AIM) study was made. AIM analysis plays an important role to explicate the electron distribution in molecules and identify the special properties of the same. Based on total electron density, the molecular structure and the bonds are analyzed. The molecular graphs of the systems were analyzed to calculate the abundance and types of noncovalent interactions. The NCI and AIM were calculated at the M06–2X-D3/6–31 G(d,p) level of theory, using the Multiwfn software [66]. To interpret the chemical bonding, NBO (Natural Bond Orbital Analysis) [67,68] was used, and was performed using the NBO 6.0 [69]. Molecular visualization of the systems was carried out with the VMD software package [70].

The assessment of kinetic stability was conducted through molecular dynamic simulations employing the semi empirical tight-binding method. The GFN2-xTB Hamiltonian with GBSA implicit solvation model of water was utilized for all simulations[71,72] A duration of 1.6 nanoseconds was set for the simulations of each AC/CECs system. During these simulations, the equations of motion were integrated using a time step of 4.0 femtoseconds within the constant number of atoms, constant volume, and constant temperature (NVT) ensemble at a temperature of 298.15 K. To maintain this constant temperature, a Berendsen thermostat was employed. The SHAKE algorithm was applied to ensure the stability of all hydrogen atoms [73]. Data were recorded every 10 femtoseconds throughout the molecular dynamic runs.

3. Results and discussion

3.1. Molecular electrostatic potential maps

Fig. 1 provides a visual representation of electrostatic potential energy that can help predict the sites of nucleophilic attack, electrophilic attack, or areas prone to chemical bonding. In these maps, different colors are observed, where the red represents the zone with the negative potential of Molecular Electrostatic Potential (MEP), associated with reactive electrophilic sites, and the blue color is adapted to the zone with the positive potential and represents the suitable center of the nucleophilic attacks. Hence, it was possible to analyze the potential interaction sites responsible for the formation of bonds by evaluating the proton donors and acceptors in each molecule. For example, ATZ has five interaction sites, two of which are proton donors and the others are proton acceptors. In the case of IBU, the electron density is more localized on the carboxylate group of the molecule, which could interact with the electron-poor peripheral atoms of the AC surface.

3.2. Analysis of Kick-Fukui potential energy surface

A comprehensive exploration of the Potential Energy Surface (PES) of the ATZ, CAF, CBZ, IBU, and SMX pollutants on the AC surface in their singlet state was carried out. To carry out this investigation, models based on DFT in its conceptual approach were employed, together with a molecular fragment assembly methodology to expand the system to a larger scale (Kick-Fukui method). The molecular fragment assembly strategy was designed using the chemical potential as a criterion, which allowed the identification of specific molecular fragments that acted as nucleophiles or electrophiles in the system. The Fukui Function (FF) played a key role in pinpointing regions of increased reactivity in the context of nucleophilicity and electrophilicity. For a more precise understanding of reactivity, a detailed analysis involving quantification of the most reactive areas was carried out. This quantification was based on Fukui function condensation, providing quantitative values that highlight the region's most likely to react. In terms of the assembly strategy, the molecular fragments were strategically oriented to meet the *Maximum Matching* [33] criterion, thus maximizing coherence and congruence in the assembly process.

Using the combination of conceptual DFT and the molecular fragment assembly approach (Kick-Fukui method), we succeeded in comprehensively investigating the PES of ATZ, CAF, CBZ, IBU, and SMX pollutants on the surface of AC in the singlet state. All this is to explore the adsorption behaviors of pollutants on the AC surface, including different configurations (see Figures S1-S5 in Supplemental Material). Our results provide valuable information on the most reactive sites and the nucleophilic and electrophilic interactions in this system, which have significant implications for the design and understanding of reactions at molecularly complex interfaces. In this context, we have obtained putative global minima for AC/CECs systems. The graphical representation of these global minima is presented in Fig. 2. Analyzing this figure, a distinctive pattern is observed concerning the electron-donating or electron-attracting nature of the compounds, as well as

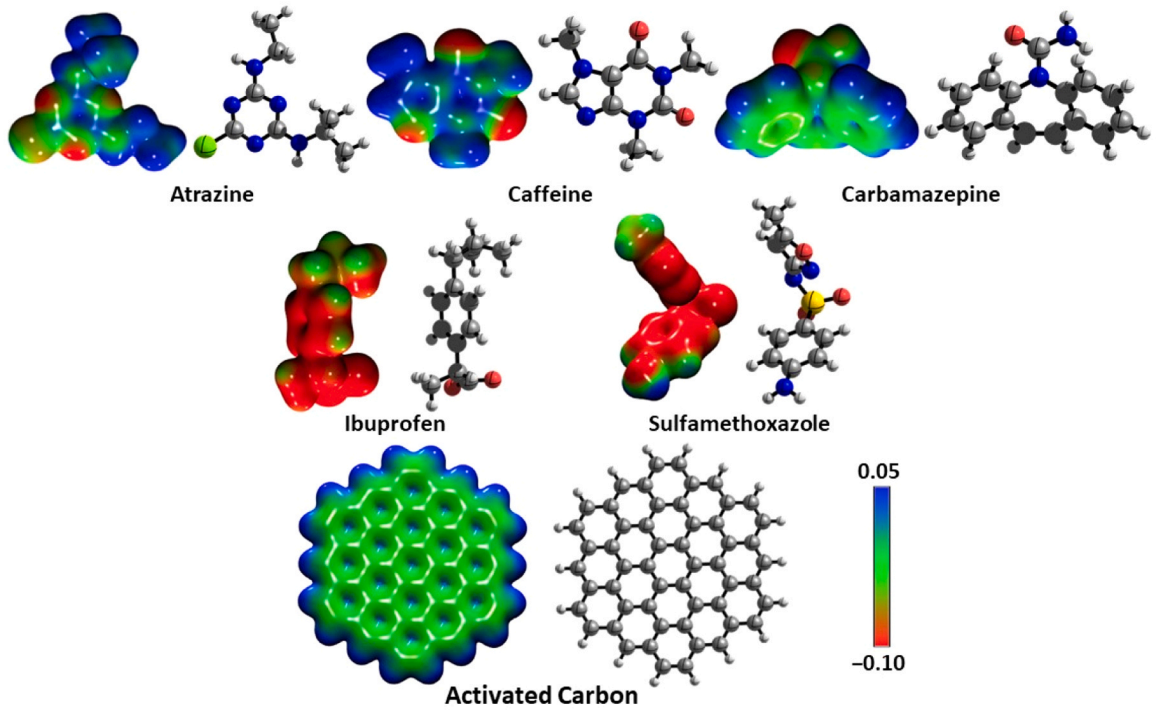

Fig. 1. Schematic representations of Molecular Electrostatic Potential (MEP) surfaces (0.01 a.u.) for ATZ, CAF, CBZ, IBU, SMX, and AC molecules computed at the M06–2X-D3/6–31 G(d,p) level of theory. Color-coded with red representing electron-rich or partially negative regions, blue indicating electron-deficient or partially positive regions, and green for slightly electron-rich regions. Color coding: red = oxygen, blue = nitrogen, gray = carbon, white = hydrogen, chlorine = green and sulfur = yellow.

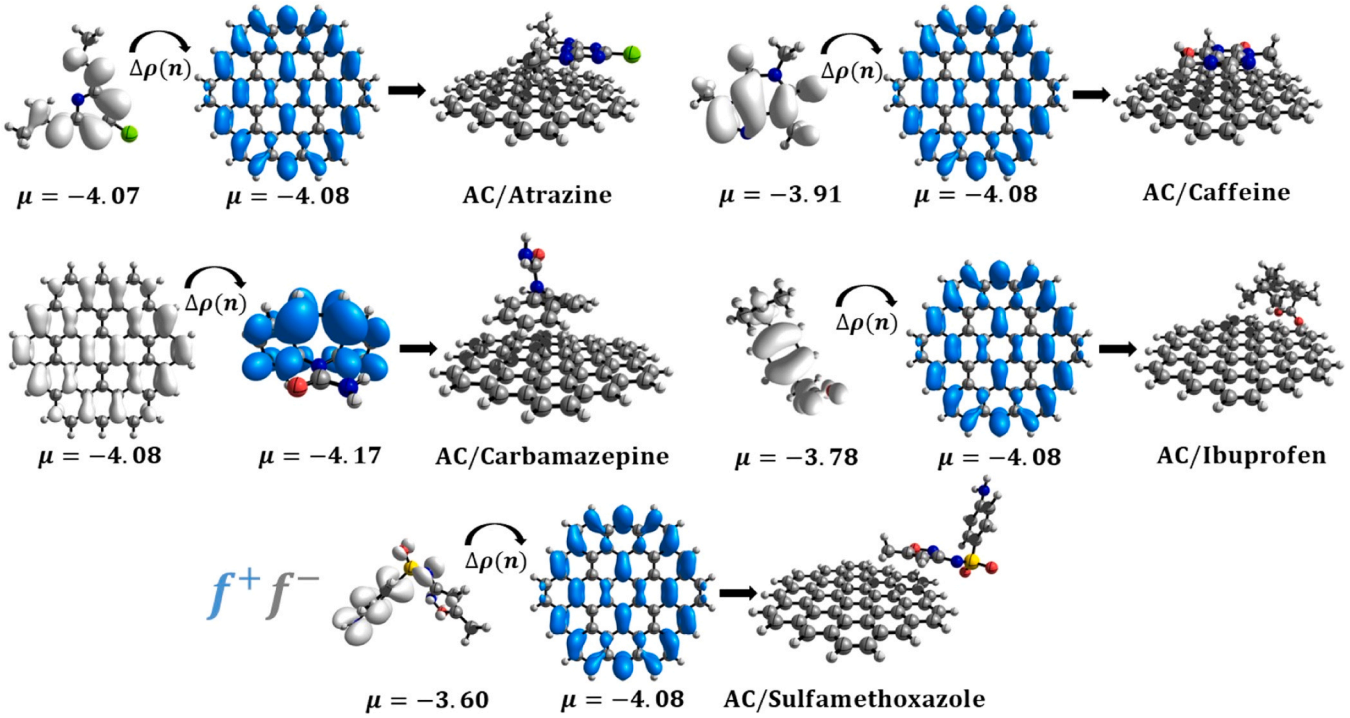

Fig. 2. Fukui function (FF) isosurfaces (0.018 a.u.) and condensed values of putative global minimum structures of AC/CECs systems. f^- represents the FF for the electrophilic attack and f^+ represents the FF for the nucleophilic attack. S.

their interaction with the AC surface. Specifically, compounds ATZ, CAF, IBU, and SMX exhibit electro-donating behavior, while the AC surface acts as an electro-attractant. In contrast, the CBZ compound shows the opposite behavior, being an electro-attractant in the presence of the AC surface, which in turn acts as an electron donor. This phenomenon is intrinsically related to the chemical potential calculated for each molecular fragment.

Our PES analysis has yielded crucial results on the arrangement and

interactions of ATZ, CAF, CBZ, IBU, and SMX pollutants on the AC surface. ATZ, CAF, and CBZ pollutants have been identified and positioned at the center of the AC surface. This strategic location allows them to interact significantly with the aromatic rings present. The presence of these interactions with the aromatic rings suggests a particular affinity between these pollutants and the aromatic regions on the AC surface. On the other hand, IBU and SMX pollutants, have been located at the edge of the AC surface. This more peripheral position facilitates their interaction with the terminal carbons and hydrogens of the aromatic rings. This position can be attributed to the negative charge that these pollutants possess at neutral pH. The electrostatic repulsion between the negative charge of the pollutants and the negative partial charges on the terminal carbons and hydrogens could influence this preferential location.

In the analyzed AC/CECs systems, relative energies between the nearest local minima range between 0.01 and 3.15 kcal/mol. It has been identified that the nearest local minimum in terms of relative energy in the AC/ATZ system has a value of 0.05 kcal/mol, while in the AC/CAF and AC/IBU systems, these values are 0.01 kcal/mol, respectively. The AC/SMX system exhibits a value of 0.41 kcal/mol, and in the AC/CBZ system, the nearest local minimum in relative energy is distinguished by its higher value of 3.15 kcal/mol. These results capture the variability in the relative stability of the local minima of the studied systems, providing essential information for understanding the interaction characteristics and their molecular conformation. The local minima with the highest relative energy represent configurations vertical concerning the AC plane. Thus, these results indicate that the parallel configuration, representative of the lower energy's adsorption systems, is more stable, which also would mean that the interaction process between the selected pollutants and AC is mainly physical adsorption. These findings have important implications in the optimization and design of processes involving the interaction between pollutants and AC surface.

3.3. Global chemical reactivity descriptors

The HOMO-LUMO energy gap ($\Delta E_{H\text{-}L}$) refers to the difference in energy between the highest occupied molecular orbital (HOMO) and the lowest unoccupied molecular orbital (LUMO) in a molecule. This $\Delta E_{H\text{-}L}$ plays a crucial role in determining the excitability and properties of a substance. A smaller $\Delta E_{H\text{-}L}$ indicates a higher propensity for excitations, which can affect the substance's characteristics. In the context of the AC/CECs systems (Table 1 and Figure S6 in Supplemental Material), the $\Delta E_{H\text{-}L}$ ranges from 4.32 eV to 4.34 eV, showing a remarkable similarity among the various systems. This similarity in energy gaps suggests that the electronic properties and reactivity of these systems are closely related.

The chemical potential (μ) is a parameter that quantifies the tendency of electrons to escape from an equilibrium system. It represents the energy that can be absorbed or released due to a change in the particle number of a given species, such as in a chemical reaction or phase transition. The μ is related to the Gibbs free energy (ΔG), which is a thermodynamic potential that measures the maximum reversible work that may be performed by a system at constant temperature and pressure. In the context of the selected AC/CECs systems, the μ values range from −3.81 eV to −3.87 eV, which as shown by $\Delta E_{H\text{-}L,}$ highlights a remarkable similarity among the selected species, in this case, regarding their electron escape tendency. The higher μ-values of the AC/CAF (3.87 eV), AC/ATZ (3.86 eV), and AC/CBZ (3.85 eV) systems suggest that these systems have a slightly lower propensity to undergo phase changes, chemical reactions, or other processes that may affect their stability. This hints at a more pronounced inclination of these systems to undergo transitions between different phases, to react with other surrounding substances, or to exhibit lower susceptibility. This lower or greater susceptibility to change could influence their behavior and performance under various conditions.

Chemical hardness (η) is a metric that gauges the stability of a chemical system, with higher values indicating increased stability. It is defined as the resistance towards electron transfer or structural changes in a chemical species. Pearson's absolute hardness can be calculated as half the second derivative of a species' energy concerning changes in the total number of electrons. In this context, η is a metric gauging the stability of an AC/CECs system and is associated with higher values indicating heightened stability. Within the dataset furnished, the η values range from 2.17 eV to 2.18 eV, emphasizing the congruence in the stability of the AC/CECs systems under scrutiny. This range suggests that the systems have similar resistance to electron transfer or structural changes, which is essential for their effectiveness in adsorbing and removing pollutants. In addition, it is worth mentioning that all systems have a positive ν_{min}, which is presented as a putative global minimum.

Table 1
Some global descriptors, HOMO-LUMO energy gaps, and smallest vibrational frequencies for the AC/CECs systems.

System	E_{HOMO}[a]	E^{a}_{LUMO}	$\Delta E_{H\text{-}L}$[a]	Chemical Potential (μ)	Chemical hardness (η)	ν^{b}_{min}
AC/ATZ	−6.03	−1.69	4.34	−3.86	2.17	23
AC/CAF	−6.04	−1.69	4.34	−3.87	2.18	27
AC/CBZ	−6.01	−1.68	4.32	−3.85	2.17	9
AC/IBU	−5.99	−1.65	4.34	−3.82	2.17	14
AC/SMX	−5.98	−1.64	4.33	−3.81	2.17	11

[a] in eV. [b] in cm^{-1}.

3.4. Thermodynamic properties analysis

The specific interactions between AC and CECs can be attributed to various factors, such as the molecular structures and physicochemical properties of the pollutants, as well as the surface properties of AC. Some possible interactions between pollutants and AC include π-stacking, hydrogen bonding, and van der Waals forces. The efficiency and selectivity of AC as an adsorbent for pollutants depend also on its physicochemical properties, such as high porosity, high surface area, and the presence of functional groups on its surface [74]. The presence of surface oxygenated groups on AC can increase surface polarity, which in turn affects the interactions with pollutants. Heat treatment of AC can be used to remove oxygenated chemical groups and modify their surface chemistry, and thus influence the adsorption process. The differences in thermodynamic properties among the AC and pollutant systems can provide insights into the efficiency and selectivity of AC for the removal of these pollutants. The analysis of the thermodynamic properties of the AC and pollutant systems revealed several trends. Table 2 presents the changes in binding energy (ΔE), enthalpy (ΔH), Gibbs free energy (ΔG), and entropy (ΔS) for each system.

The AC/CAF and AC/ATZ combination displayed the most notable outcomes in terms of thermodynamic parameters, showcasing the most profound alterations in ΔE with values of −24.1 kcal/mol and −20.3 kcal/mol respectively. Similarly, the ΔH exhibited substantial shifts, registering as −24.5 kcal/mol (AC/CAF) and −20.2 kcal/mol

Table 2
Thermodynamic properties at the M06-2X-D3/6–31 G(d,p) level of theory, for the AC/CECs systems.

Systems	ΔE^{a}	ΔH^{a}	ΔG^{a}	ΔS^{b}
AC/ATZ	−20.3	−20.2	−5.6	−48.9
AC/CAF	−24.1	−24.5	−8.9	−52.1
AC/CBZ	−17.5	−17.5	−4.0	−45.2
AC/IBU	−15.9	−14.9	−4.2	−35.9
AC/SMX	−11.9	−11.4	0.7	−40.6

[a] in kcal/mol. [b] in cal/mol*K.

(AC/ATZ). These interactions also induced substantial modifications in ΔG, measuring at −8.9 kcal/mol and −5.6 kcal/mol for AC/CAF and AC/ATZ, respectively. Additionally, the ΔS changes stood at −52.1 cal/mol*K (AC/CAF) and −48.9 cal/mol*K (AC/ATZ), underlining the profound impact of these combinations on thermodynamic properties when compared to other systems under study.

Scrutiny of the ΔE and ΔH changes of the AC/ATZ and AC/CBZ interactions, reveals remarkable similarities. Specifically, the alterations observed in ΔE were −20.3 kcal/mol (AC/ATZ) and −17.5 kcal/mol (AC/CBZ), while their ΔH changes were −20.2 kcal/mol for AC/ATZ and −17.5 kcal/mol for AC/CBZ. In contrast, an examination of the ΔG unveils an intriguing distinction. The ΔG change for the AC/ATZ pairing exhibited a lower value of −5.6 kcal/mol, in comparison to the AC/CBZ system which registered a value of −4.0 kcal/mol. This discrepancy suggests a more energetically favorable state for the AC/ATZ interaction, underscoring its thermodynamic stability when contrasted with the AC/CBZ interaction. Overall, while the ΔE and ΔH appear analogous for the AC/ATZ and AC/CBZ systems, the discernible divergence in ΔG points towards a differential energetic preference between the two interactions.

Analyzing the AC/IBU and AC/SMX systems, it becomes evident that these interactions manifest the most substantial values in terms of ΔE and ΔH alterations, registering at −15.9 kcal/mol and −11.9 kcal/mol for AC/IBU, and −14.9 kcal/mol and −11.4 kcal/mol for AC/SMX. These results suggest that the introduction of IBU and SMX to the AC framework induces relatively minimal shifts in ΔE and ΔH parameters. This indicates that the interactions between AC and these two compounds lead to relatively modest changes in the overall energy content of the system. Furthermore, the AC/SMX system stands out as a unique case within this study due to its positive ΔG value of 0.7 kcal/mol. This positive value carries significant thermodynamic implications. Specifically, it signifies that the adsorption process of SMX onto AC is not thermodynamically favorable under the specified conditions. In other words, the forces driving the interaction between AC and SMX do not align with the prevailing thermodynamic tendencies, making the adsorption of SMX onto AC less energetically advantageous compared to other systems *i.e.* AC/ATZ, AC/CAF, or AC/CBZ.

3.5. AC/CECs system interactions based on Morokuma-Ziegler analysis

The analysis using the EDA scheme was done to achieve a deeper understanding of these AC/CECs interactions. In all cases, the interaction energy (ΔE_{Int}) was computed considering two fragments: AC and pollutants. The interaction energy AC/CECs were between −17 kcal/mol and −26 kcal/mol, as can be seen in Table 3. According to the calculations, the interaction energy for AC/ATZ was −20.87 kcal/mol. This result revealed that the dispersive forces that act between the AC/ATZ are relevant. For this system, specifically, the dispersion component represented 60% of the total stabilizing energy.

Electrostatic interaction ($\Delta E_{Elestat}$) and orbital interaction (ΔE_{Orb}) each contribute 23% and 17% of the total stabilizing energy. Similar trends were found for CBZ and CAF, as shown in Table 3, which were $\Delta E_{Int} = -20.62$ and −17.05 kcal/mol, respectively. In each system, the ΔE_{Disp} accounts for 60% of the total stabilizing energy in AC/CBZ, and AC/CAF systems.

Table 3
Morokuma-Ziegler scheme energy decomposition analysis (EDA), values in kcal/mol, for the AC/CECs interacting systems.

System	ΔE_{Pauli}	$\Delta E_{Elestat}$	ΔE_{Orb}	ΔE_{Disp}	ΔE_{Int}
AC/ATZ	28.82	−11.71 (23%)	−8.21 (17%)	−29.77 (60%)	−20.87
AC/CAF	20.18	−8.72 (23%)	−6.30 (17%)	−22.20 (60%)	−17.05
AC/CBZ	33.81	−12.99 (24%)	−8.80 (16%)	−32.64 (60%)	−20.62
AC/IBU	20.08	−11.99 (26%)	−15.66 (34%)	−18.14 (40%)	−25.71
AC/SMX	16.50	−7.77 (22%)	−12.65 (35%)	−15.52 (43%)	−19.45

The results also revealed that the $\Delta E_{Elestat}$ and ΔE_{Orb} that act between the AC/CBZ, represented 24% and 16% of the total stabilizing energy. In the case of the AC/CAF system, the calculation indicates that the contribution to the $\Delta E_{Elestat}$ and ΔE_{Orb} are 23% and 17% percent, respectively. Therefore, in each of these three systems, the dispersion interactions have the main contributions to forces acting between AC and pollutants (ATZ, CBZ, and CAF). Whereas, in the case of AC/SMX and AC/IBU systems, interaction energies were −19.45 kcal/mol and −25.71 kcal/mol, respectively. These ΔE_{Int} fall in the same range of values of AC/ATZ, AC/CBZ, and AC/CAF. Calculations reveal that for AC/SMX and AC/IBU, the dispersive component contributes 40% and 43%, respectively of the total stabilizing energy. Mainly the contribution ΔE_{Elec} component represents 22% and 26%, respectively, of the total attractive energy, see Table 3.

Although in all cases the dispersive component is the term that makes the greatest contribution to the stabilizing energy, the results also show that the molecular conformation that the pollutants adopted concerning the AC surface plays an important role in the intermolecular interactions. In the case of ATZ, CAF, and CBZ which adopt a parallel conformation positioned at the center of the AC surface, the ΔE_{Disp} term constitutes 60% of the stabilizing energy. However, in the case of IBU and SMX pollutants, which assumed a conformation in a more peripheral position, *i.e.*, towards the edge of the AC surface, the ΔE_{Disp} term constitutes 40–43% of the total interaction energy, somewhat less than the results obtained for AC/ATZ, AC/CAF, AC/CBZ. In addition to the molecular conformation, the molecular structure of these pollutants, with aromatic rings, the presence of heteroatoms, functional groups, and aromatic regions on the AC surface, presumably influence the dispersion, a factor that plays a decisive role in stabilizing all the complexes. Thus, the next step was to investigate the interactions between AC and pollutants using other methods discussed below.

3.5.1. Natural orbital chemical valence analysis

An analysis based on the NOCV methodology proposed by Mitoraj and Michalak [61,75] was carried out, to explore in detail the channels of donor-acceptor interaction between AC and the pollutants. For the AC/ATZ system, the donor-acceptor interaction is formed between AC and the ATZ molecule, see Fig. 3, top-left image. The deformation density channels show that these interactions involved a donation of the lone pair of nitrogen of the ATZ molecule, to the AC moieties. In the case of AC/CAF, the NOCV analysis also indicated that the deformation density channel, $\Delta\rho$ originated predominantly from the electron donation from CAF to AC, see Fig. 3, top-right image. For this system, the deformation density channels evidence a charge depletion (outflow) that involved the heteroatoms of CAF, whereas an accumulation (inflow) of electron density arose in the region of AC. The bottom-left image in Fig. 3 illustrates the NOCV deformation density contributions for the AC/CBZ system. The complementary pairs of NOCVs describe deformation density contributions π-networks $\Delta\rho(\pi)$ in aromatic regions both on the CBZ and the AC surface. This can be associated with the probable π···π stacking interaction between AC and CBZ. This finding aligns well with the analysis conducted using conceptual DFT and the Kick-Fukui method discussed earlier. In addition, these results are also consistent with the EDA analysis for these three pollutants, *i.e.*, ATZ, CAF, and CBZ, regarding the dominant dispersive contribution previously discussed. Finally, in the case of the AC/IBU (bottom-center image) and AC/SMX (bottom-right image) in Fig. 3, the contours of deformation densities also display the probable molecule-to-surface charge flow. However, unlike the other three systems analyzed, for these two systems no evidence that the donation or back-donation channels originate from the electron donation. These theoretical results strongly suggest that the nature of intermolecular interactions

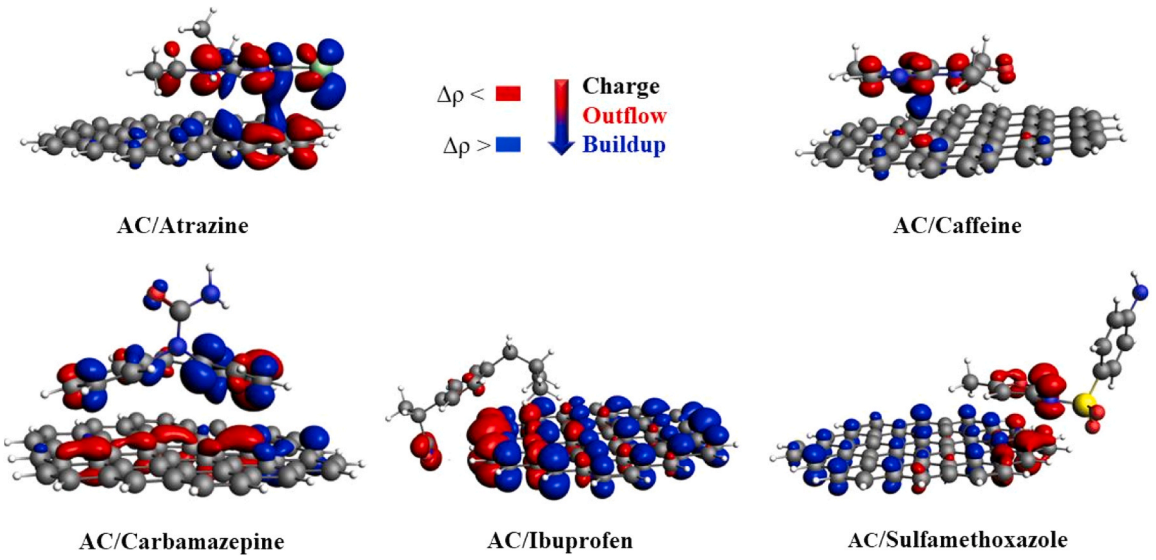

Fig. 3. Contours of deformation density channels (Δρ), which describes the intermolecular interactions AC/CECs systems. Red and blue contours represent a depletion (outflow) and accumulation (inflow) of electron density, respectively. Color coding: red = oxygen, blue = nitrogen, gray = carbon, white = hydrogen, chlorine = green and sulfur = yellow.

between AC/pollutants has an important role in the adsorption process of these molecules on AC.

3.6. Non-covalent interaction index

The interactions between AC and pollutants are governed by a combination of factors, including the molecular structures and

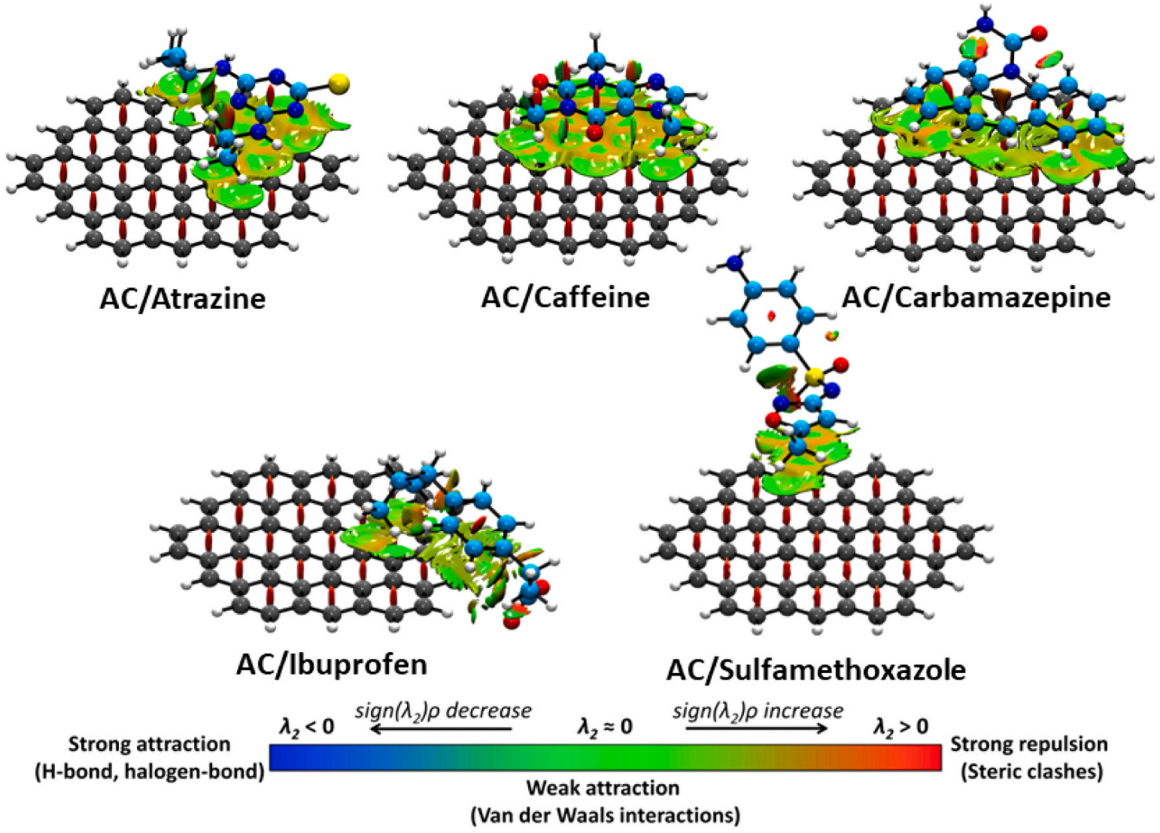

Fig. 4. NCI plot isosurfaces (0.6 a.u.) to visualize non-covalent interactions in AC/CECs systems. The sign of λ_2 enables the identification of the interaction type. Attractive interactions appear at $\lambda_2 < 0$ whereas in the cases where λ_2 is positive (as in rings or cages), usually several atoms interact but are not bonded, which corresponds to steric crowding according to classical chemistry. The blue regions indicate pronounced attractive interactions, whereas the green regions indicate relatively weaker interactions. Color coding: red = oxygen, blue = nitrogen, gray = carbon (AC fragment), cyan = carbon (CECs), white = hydrogen, chlorine = green and sulfur = yellow.

physicochemical properties of the pollutants, as well as the surface properties of AC. These interactions are characterized by non-covalent interactions such as π-stacking and van der Waals forces. To distinguish between attractive and repulsive interactions, we examine the second derivatives of the density along the principal axis of variation. The second eigenvalue (λ_2) can be either positive or negative, depending on the type of interaction. On the one hand, binding interactions, such as H…H interactions, are characterized by $\lambda_2<0$, and density accumulation perpendicular to the bond. Non-binding interactions, such as steric repulsion, produce density depletion, so $\lambda_2 > 0$. The troughs in the range of close to zero correspond to the weak C–H…π, London forces as in π-π interactions and dispersion H…H interactions, represented in green in the isosurface [64]. Fig. 4 shows the NCI analysis, where for each AC/CECs system, the most important intramolecular interactions that provide stabilization are the van der Waals interactions. So, the van der Waals interactions are responsible for stabilizing the CECs on the AC surface. These interactions are more intense when the contact area between the CECs and AC is larger. Visually, it can be observed that the largest areas of interaction are presented by the AC/ATZ, AC/CAF, and AC/CBZ systems. Therefore, it is possible to suggest that the adsorption process would be more favored in these systems. Each contaminant exhibits unique non-covalent interactions with AC, influencing their adsorption mechanisms. ATZ adsorption onto AC involves multiple mechanisms, such as electrostatic interactions, van der Waals forces, hydrophobic interactions, and π-π electron donor–acceptor interactions. CAF adsorption on AC is influenced by various factors, including non-covalent interactions like π-π interactions and hydrophobic interactions. Previously, it was experimentally reported that the adsorption capacity of CAF and IBU on AC is mainly related to the value of the octanol-water partition coefficient (log Kow) linked to hydrophobic interactions [76]. The adsorption behavior of CBZ is mainly influenced by the surface chemistry of the adsorbent. The main identified mechanisms that contribute to CBZ adsorption include π-π interactions with the adsorbents possessing aromatic rings in their composition. IBU binds to AC mainly through non-covalent interactions, including van der Waals forces between the carboxyl group of IBU, while the SMX adsorption on AC is primarily driven by non-covalent forces, such as van der Waals forces, hydrophobic interactions, and π-π electron donor–acceptor interactions. This type (π-π EDA) of interaction was found to be an important driving force for the sorption of CECs on AC surfaces in several studies reported earlier [29–32].

The interaction force between CECs and AC was visualized using the IGMH approach to analyze both its type and interaction regions. The mapping function in the IGMH evidences type of interactions utilizes color coding. The green area symbolizes van der Waals interactions, the blue area signifies the potential to create hydrogen bonds, and the red area mirrors a repulsive interaction.[77] Fig. 5 provides a visual representation of the adsorption pattern of CECs on the AC plane, clearly showcasing a predominance of dispersion occurring between the aromatic rings of CECs and the aromatic areas on the AC surface. As per the IGMH map, the green isosurfaces predominantly entail π–π stacking interactions between the aromatic rings of CECs on the AC.[78] [79] Therefore, the intermolecular interaction in these systems is mainly governed by the dispersive forces that act between the AC/CECs. This results clearly evidenced that the simulation of the host-guest system is imperative to understand mechanisms involved in the adsorption of CECs on AC. Overall, these results are in good agreement with the other approaches used for analyzing the intermolecular interactions described

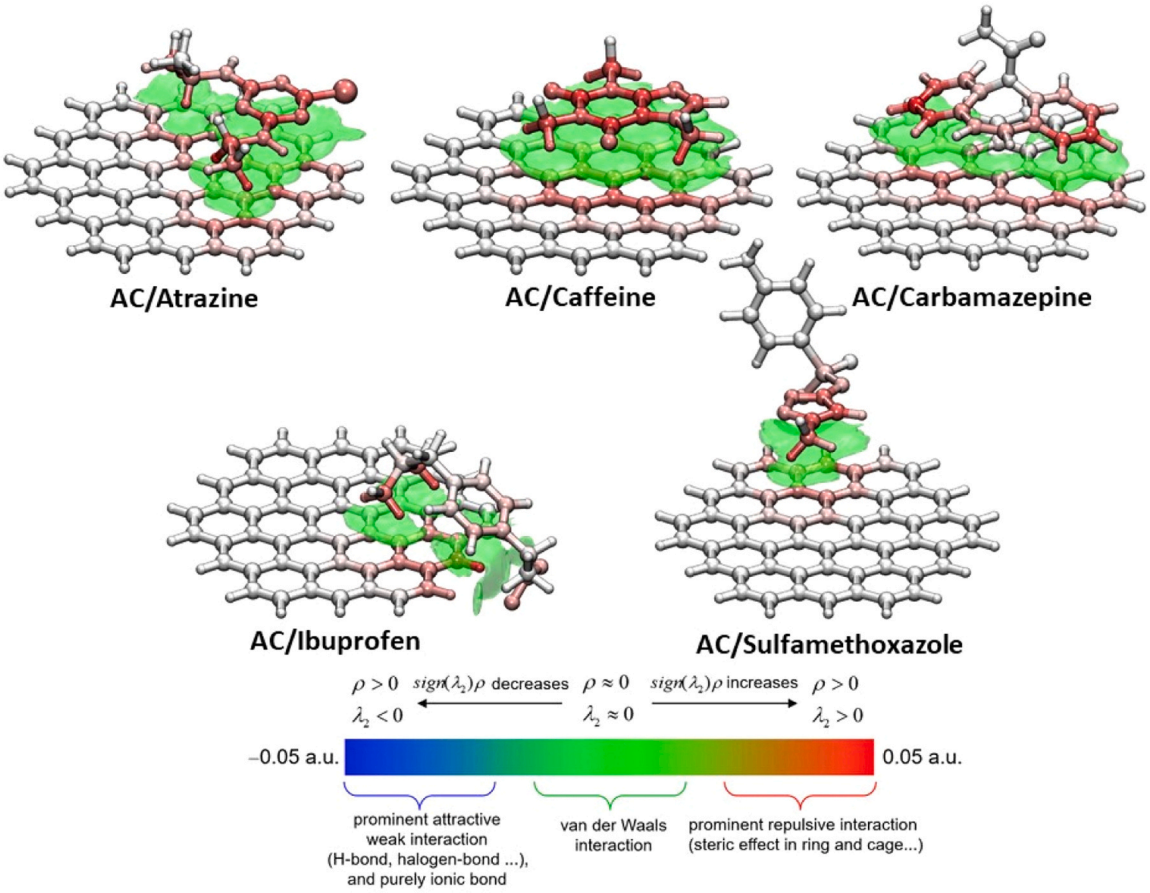

Fig. 5. IGMH analysis (δg^{inter}=0.003 a.u.) of AC/CECs systems at M06–2X-D3/6–31 G(d,p) level of theory. The prominent van der Waals interaction zone, specifically the π-π stacking region, is depicted by the green isosurface. The atoms colored in shades of red denote a higher degree of contribution to this interaction. Color coding: red = oxygen, blue = nitrogen, gray = carbon (AC fragment), cyan = carbon (CECs), white = hydrogen, chlorine = green and sulfur = yellow.

in the previous section.

Atoms The study of Atoms in Molecules (AIM) analysis is crucial for elucidating the electron distribution within molecules and discerning their unique properties. AIM analysis primarily revolves around examining the total electron density within a molecule to gain insights into its molecular structure and the nature of its chemical bonds. A key aspect of AIM analysis involves investigating the topology parameters of AC/CECs systems. These parameters provide valuable information about the spatial distribution of electron density within the molecule. Fig. 6 illustrates the analysis results, presenting the positions of all bond critical points (BCPs), denoted by coordinates such as (3,+3), (3,+1), and (3,-1). These BCPs signify regions where significant electron density gradients occur, indicating the presence of π-π stacking, and van der Waals interactions. Additionally, the figure depicts the bond paths connecting different components of the molecule. In addition, a topological study was carried out for AC/CECs (see Table S1): Density of all electrons, Hamiltonian kinetic energy, Potential energy density, Energy density, Laplacian of electron density, Lagrangian kinetic energy, Ellipticity of electron density, Sign(λ_2)*rho, and Delta-g (under Hirshfeld partition), The values in this table offer deep insights into the fundamental nature of π-π stacking, and van der Waals interactions by dissecting the topology and properties of the electron density distribution in the AC/CECs.

3.7. Natural population analysis charge analysis

The investigation of charge distribution is crucial for understanding the electronic properties of the AC/CECs systems. To achieve precise charge values, the NBO method for Natural Population Analysis (NPA) charges was applied, as shown in Fig. 7. Charge transfer occurs when atoms redistribute their charges, generating distinct potential fields. A positive charge indicates outward electron flow, while a negative charge reflects inward electron flow. In the context of AC/CECs systems, NPA analyses can help to understand the non-covalent interactions between AC and the pollutants, which as mentioned before, are influenced by the molecular structures and physicochemical properties of the pollutants, as well as the surface properties of AC. By utilizing the NPA method, it is possible to obtain precise charge values for the atoms in the pollutants and AC, which can provide a better understanding of the interactions between them.

Fig. 7 provides valuable insights into the charge distribution within stable AC/CECs structures. The NPA charge values for AC/ATZ range between −0.71 and 0.66 a.u. These values suggest that there is a moderate charge transfer between AC and ATZ, which could be attributed to various non-covalent interactions such as electrostatic interactions, and π-π electron donor-acceptor interactions. The NPA charge values for AC/CAF range between −0.66 a.u. and 0.86 a.u. This range indicates a relatively strong charge transfer between AC and CAF, which could be due to non-covalent interactions like π-π interactions, and hydrophobic interactions. The strong charge transfer may contribute to the high adsorption efficiency of AC for CAF, as observed in the thermodynamic properties. The NPA charge values for AC/CBZ range between −0.91 a.u. and 0.85 a.u. This range suggests a significant charge transfer between AC and CBZ, which could be due to π-π interactions with the adsorbents possessing aromatic rings in their composition. The NPA charge values for AC/IBU range between −0.80 a.u. and 0.81 a.u. indicating a moderate charge transfer between AC and IBU, which could be due to non-covalent interactions such as van der Waals forces between the carboxyl group of IBU and the AC. The moderate charge transfer may be related to the higher ΔG value observed for the AC/IBU system, suggesting that the adsorption of IBU on AC is not thermodynamically favorable. Similarly, the NPA charge values for AC/SMX range between −1.05 a.u. and 2.41 a.u. This wide range of values indicates a strong charge transfer, which could be driven by non-covalent interactions such as van der Waals forces. Also, may be related to the positive ΔG value observed for the AC/SMX system, suggesting that the adsorption is not thermodynamically favorable.

3.8. Tight-binding molecular dynamics simulations

To analyze the kinetic stability of the pollutants on the AC surface and to evaluate the methodology used, Tight-binding molecular dynamics calculations were performed for all systems. In general, lower RMSD values indicate that the atomic positions in the compared structures are more similar, while higher RMSD values indicate greater differences between the structures in the simulations performed. Fig. 8 shows that the RMSD (Root Mean Square Deviation) fluctuation is very low at 298.15 K for ATZ, CAF, and CBZ on AC, averaging 0.75 Å, 0.13 Å, and 0.23 Å, respectively. These results indicate that ATZ, CAF, and CBZ are kinetically stable. On the other hand, in the AC/IBU and AC/SMX systems, with an average of 1.28 Å and 1.54 Å, the RMSD fluctuation is

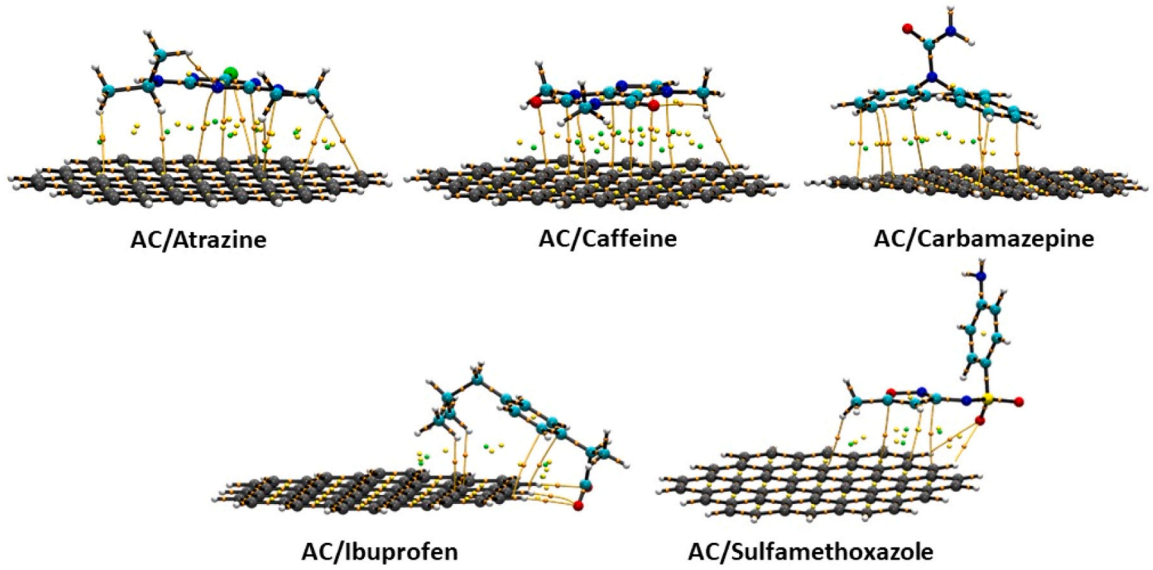

Fig. 6. AIM molecular graph showing the different Bond Critical Points (BCPs) of AC/CECs systems. Green, yellow, and orange spheres in the above map correspond to (3,+3), (3,+1), and (3,−1) critical points, respectively. Brown lines denote bond paths. Color coding: red = oxygen, blue = nitrogen, gray = carbon (AC fragment), cyan = carbon (CECs), white = hydrogen, chlorine = green and sulfur = yellow.

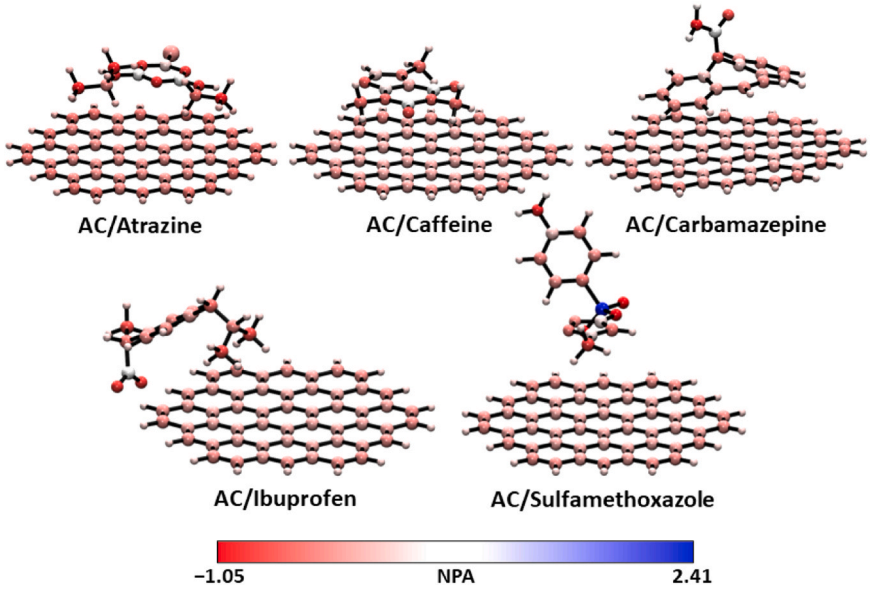

Fig. 7. NPA charge values for AC/CECs systems. The color code of atoms corresponds to the NPA charge values.

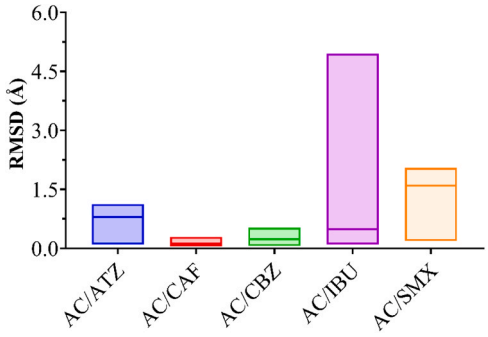

Fig. 8. Floating bar plots of Root-mean-square deviation (RMSD) from tight-binding molecular dynamics simulations of AC/CECs systems.

higher, suggesting that they are kinetically less stable. Although RMSD values $\leq$ 2 Å are considered reasonably good according to Xiao et al. [80], in these simulations, high values represent reduced kinetic stability. In the case of the IBU system in AC, around 200 ps of the simulation (see **SV4** in Supporting Information), a decarboxylation reaction occurs, releasing the carboxyl group from the main IBU backbone in the form of CO_2. Therefore, it is possible to state that the interactions of ATZ, CAF, and CBZ in AC are maintained over time, indicating kinetic stability provided by aromatic interactions.

4. Conclusions

In this article, we develop a theoretical protocol that offers a valuable tool for examining five AC/CECs systems, allowing us to better understand the interactions and adsorption between AC and CECs. Molecular electrostatic potential maps, conceptual density functional theory, Fukui functions, and thermodynamic analysis provided insights into the electronic/energetics interactions, and mechanisms involved in AC adsorption of CECs.

- Thermodynamic analysis for all systems reveals adsorption may be unfavorable for AC/IBU and AC/SMX systems compared to the other study systems.
- The pollutants' molecular conformation on the AC surface significantly impacts intermolecular interactions.
- Interactions between AC and CECs include π-stacking, hydrogen bonding, van der Waals forces, and hydrophobic/electrostatic interactions.
- Simulations through tight-binding molecular dynamics indicating some CECs are kinetically stable on the activated carbon surface, in the following order CAF (0.13 Å)>CBZ (0.23 Å)>ATZ (0.75 Å)> IBU (1.28 Å)>SMX (1.54 Å).

CRediT authorship contribution statement

Yoan Hidalgo- Rosa: Writing – original draft, Software, Methodology, Investigation. **Karel Mena- Ulecia**: Investigation. **Osvaldo Yañez**: Writing – original draft, Validation, Software, Methodology, Investigation, Data curation. **Lisdelys González- Rodríguez**: Methodology, Investigation, Formal analysis. **Claudia Ulloa-Tesser**: Writing – review & editing, Supervision, Conceptualization. **Ximena García**: Writing – review & editing, Conceptualization.

Declaration of Competing Interest

The authors declare that they have no known competing financial interests or personal relationships that could have appeared to influence the work reported in this paper.

Data availability

Data will be made available on request.

Acknowledgments

This research work has been supported by the ANID/FONDEF/ID22I10006 and ANID/FONDAP/1523A0006 projects. L.G.-R. and O. Y.-O. gratefully acknowledge the NIDS (https://nids.cl). Y.H-R is grateful for the ANID Postdoctoral 3230141. Powered@NLHPC: This research was partially supported by the supercomputing infrastructure of the NLHPC (ECM-02) of the Universidad de Chile.

Appendix A. Supporting information

Supplementary data associated with this article can be found in the online version at doi:10.1016/j.jece.2024.112911.

References

[1] REGULATION (EU) 2020/741 OF THE EUROPEAN PARLIAMENT AND OF THE COUNCIL of 25 May 2020 on minimum requirements for water reuse (Text with EEA relevance), n.d.

[2] L. Limousy, I. Ghouma, A. Ouederni, M. Jeguirim, Amoxicillin removal from aqueous solution using activated carbon prepared by chemical activation of olive stone, Environ. Sci. Pollut. Res. 24 (2017) 9993–10004, https://doi.org/10.1007/s11356-016-7404-8.

[3] J.R. Rohr, B.D. Palmer, Aquatic herbicide exposure increases salamander desiccation risk eight months later in a terrestrial environment, Environ. Toxicol. Chem. 24 (2005) 1253–1258, https://doi.org/10.1897/04-448R.1.

[4] H. Ramézani, I. Ellien, Z. El Oufir, N. Mathieu, S. Delpeux, S.K. Bhatia, Clustering of caffeine in water and its adsorption in activated carbon: molecular simulations and experiments, Colloids Surf. A Physicochem Eng. Asp. 673 (2023) 131645, https://doi.org/10.1016/j.colsurfa.2023.131645.

[5] M. Lv, D. Li, Z. Zhang, B.E. Logan, G. Liu, M. Sun, C. Dai, Y. Feng, Unveiling the correlation of Fe3O4 fractions upon the adsorption behavior of sulfamethoxazole on magnetic activated carbon, Sci. Total Environ. 757 (2021) 143717, https://doi.org/10.1016/j.scitotenv.2020.143717.

[6] A. P, V. S, S. G, R. M, Sustainable development and analysis of a novel bio-derived (biochar) nanocomposite for the remediation of carbamazepine from aqueous solution, Chemosphere 347 (2024) 140696 https://doi.org/https://doi.org/10.1016/j.chemosphere.2023.140696.

[7] J.W. Lee, J. Han, Y.-K. Choi, S. Park, S.H. Lee, Reswellable alginate/activated carbon/carboxymethyl cellulose hydrogel beads for ibuprofen adsorption from aqueous solutions, Int J. Biol. Macromol. 249 (2023) 126053, https://doi.org/10.1016/j.ijbiomac.2023.126053.

[8] J.S. Lazarotto, K. da Boit Martinello, J. Georgin, D.S.P. Franco, M.S. Netto, D.G. A. Piccilli, L.F.O. Silva, E.C. Lima, G.L. Dotto, Application of araçá fruit husks (Psidium cattleianum) in the preparation of activated carbon with FeCl3 for atrazine herbicide adsorption, Chem. Eng. Res. Des. 180 (2022) 67–78, https://doi.org/10.1016/j.cherd.2022.01.044.

[9] M. Sgroi, S.A. Snyder, P. Roccaro, Comparison of AOPs at pilot scale: energy costs for micro-pollutants oxidation, disinfection by-products formation and pathogens inactivation, Chemosphere 273 (2021) 128527, https://doi.org/10.1016/j.chemosphere.2020.128527.

[10] C. Sheng, A.G.A. Nnanna, Y. Liu, J.D. Vargo, Removal of trace pharmaceuticals from water using coagulation and powdered activated carbon as pretreatment to ultrafiltration membrane system, Sci. Total Environ. 550 (2016) 1075–1083, https://doi.org/10.1016/j.scitotenv.2016.01.179.

[11] J.P. Gutkoski, E.E. Schneider, C. Michels, How effective is biological activated carbon in removing micropollutants? A comprehensive review, J. Environ. Manag. 349 (2024) 119434, https://doi.org/10.1016/j.jenvman.2023.119434.

[12] V. Kumar, S. Agrawal, S.A. Bhat, J.H.P. Américo-Pinheiro, S.K. Shahi, S. Kumar, Environmental impact, health hazards, and plant-microbes synergism in remediation of emerging contaminants, Clean. Chem. Eng. 2 (2022) 100030, https://doi.org/10.1016/j.clce.2022.100030.

[13] H.B. Quesada, T.P. de Araújo, L.F. Cusioli, M.A.S.D. de Barros, R.G. Gomes, R. Bergamasco, Caffeine removal by chitosan/activated carbon composite beads: adsorption in tap water and synthetic hospital wastewater, Chem. Eng. Res. Des. 184 (2022) 1–12, https://doi.org/10.1016/j.cherd.2022.05.044.

[14] M. Francoeur, C. Yacou, C. Jean-Marius, Y. Chérémond, U. Jauregui-Haza, S. Gaspard, Optimization of the synthesis of activated carbon prepared from Sargassum (sp.) and its use for tetracycline, penicillin, caffeine and methylene blue adsorption from contaminated water, Environ. Technol. Innov. 28 (2022) 102940, https://doi.org/10.1016/j.eti.2022.102940.

[15] N. Pamphile, L. Xuejiao, Y. Guangwei, W. Yin, Synthesis of a novel core-shell-structure activated carbon material and its application in sulfamethoxazole adsorption, J. Hazard Mater. 368 (2019) 602–612, https://doi.org/10.1016/j.jhazmat.2019.01.093.

[16] G. Jaria, V. Calisto, M.V. Gil, P. Ferreira, S.M. Santos, M. Otero, V.I. Esteves, Effects of thiol functionalization of a waste-derived activated carbon on the adsorption of sulfamethoxazole from water: Kinetic, equilibrium and thermodynamic studies, J. Mol. Liq. 323 (2021) 115003, https://doi.org/10.1016/j.molliq.2020.115003.

[17] M.-H. To, P. Hadi, C.-W. Hui, C.S.K. Lin, G. McKay, Mechanistic study of atenolol, acebutolol and carbamazepine adsorption on waste biomass derived activated carbon, J. Mol. Liq. 241 (2017) 386–398, https://doi.org/10.1016/j.molliq.2017.05.037.

[18] S. Bakkaloglu, M. Ersan, T. Karanfil, O.G. Apul, Effect of superfine pulverization of powdered activated carbon on adsorption of carbamazepine in natural source waters, Sci. Total Environ. 793 (2021) 148473, https://doi.org/10.1016/j.scitotenv.2021.148473.

[19] Y. Yu, D. Chen, S. Xie, Q. Sun, Z.-X. Zhang, G. Zeng, Adsorption behavior of carbamazepine on Zn-MOFs derived nanoporous carbons: defect enhancement, role of N doping and adsorption mechanism, J. Environ. Chem. Eng. 10 (2022) 107660, https://doi.org/10.1016/j.jece.2022.107660.

[20] G. Labuto, A.P. Carvalho, A.S. Mestre, M.S. dos Santos, H.R. Modesto, T.D. Martins, S.G. Lemos, H.D.T. da Silva, E.N.V.M. Carrilho, W.A. Carvalho, Individual and competitive adsorption of ibuprofen and caffeine from primary sewage effluent by yeast-based activated carbon and magnetic carbon nanocomposite, Sustain Chem. Pharm. 28 (2022) 100703, https://doi.org/10.1016/j.scp.2022.100703.

[21] M. Bouzidi, L. Sellaoui, M. Mohamed, D.S.P. Franco, A. Erto, M. Badawi, A comprehensive study on paracetamol and ibuprofen adsorption onto biomass-derived activated carbon through experimental and theoretical assessments, J. Mol. Liq. 376 (2023) 121457, https://doi.org/10.1016/j.molliq.2023.121457.

[22] Y.L. Salomón, J. Georgin, D.S.P. Franco, M.S. Netto, D.G.A. Piccilli, E.L. Foletto, D. Pinto, M.L.S. Oliveira, G.L. Dotto, Adsorption of atrazine herbicide from water by Diospyros kaki fruit waste activated carbon, J. Mol. Liq. 347 (2022) 117990, https://doi.org/10.1016/j.molliq.2021.117990.

[23] J. Lladó, C. Lao-Luque, B. Ruiz, E. Fuente, M. Solé-Sardans, A.D. Dorado, Role of activated carbon properties in atrazine and paracetamol adsorption equilibrium and kinetics, Process Saf. Environ. Prot. 95 (2015) 51–59, https://doi.org/10.1016/j.psep.2015.02.013.

[24] E.F. Mohamed, C. Andriantsiferana, A.M. Wilhelm, H. Delmas, Competitive adsorption of phenolic compounds from aqueous solution using sludge-based activated carbon, Environ. Technol. 32 (2011) 1325–1336, https://doi.org/10.1080/09593330.2010.536783.

[25] H.B. Quesada, A.T.A. Baptista, L.F. Cusioli, D. Seibert, C. de Oliveira Bezerra, R. Bergamasco, Surface water pollution by pharmaceuticals and an alternative of removal by low-cost adsorbents: A review, Chemosphere 222 (2019) 766–780, https://doi.org/10.1016/j.chemosphere.2019.02.009.

[26] U. Sarkar, D.R. Roy, P.K. Chattaraj, R. Parthasarathi, J. Padmanabhan, V. Subramanian, A conceptual DFT approach towards analysing toxicity, J. Chem. Sci. 117 (2005) 599–612.

[27] A. Vásquez-Espinal, O. Yañez, E. Osorio, C. Areche, O. García-Beltrán, L.M. Ruiz, B. K. Cassels, W. Tiznado, Structure–antioxidant activity relationships in boldine and glaucine: a DFT study, N. J. Chem. 45 (2021) 590–596, https://doi.org/10.1039/D0NJ04028B.

[28] A. Vásquez-Espinal, O. Yañez, E. Osorio, C. Areche, O. García-Beltrán, L.M. Ruiz, B. K. Cassels, W. Tiznado, Structure-antioxidant activity relationships in boldine and glaucine: a DFT study, N. J. Chem. 45 (2021) 590–596, https://doi.org/10.1039/d0nj04028b.

[29] T.N.V. de Souza, S.M.L. de Carvalho, M.G.A. Vieira, M.G.C. da Silva, D. do S. B. Brasil, Adsorption of basic dyes onto activated carbon: experimental and theoretical investigation of chemical reactivity of basic dyes using DFT-based descriptors, Appl. Surf. Sci. 448 (2018) 662–670, https://doi.org/10.1016/j.apsusc.2018.04.087.

[30] A. Spaltro, M.N. Pila, D.D. Colasurdo, E. Noseda Grau, G. Román, S. Simonetti, D. L. Ruiz, Removal of paracetamol from aqueous solution by activated carbon and silica. Experimental and computational study, J. Contam. Hydrol. 236 (2021) 103739, https://doi.org/10.1016/j.jconhyd.2020.103739.

[31] S. Muthusaravanan, K. Balasubramani, R. Suresh, R.S. Ganesh, N. Sivarajasekar, H. Arul, K. Rambabu, G. Bharath, V.E. Sathishkumar, A.P. Murthy, F. Banat, Adsorptive removal of noxious atrazine using graphene oxide nanosheets: Insights to process optimization, equilibrium, kinetics, and density functional theory calculations, Environ. Res 200 (2021) 111428, https://doi.org/10.1016/j.envres.2021.111428.

[32] R.J. Martínez, A.Z. Vela-Carrillo, L.A. Godínez, J. de J. Pérez-Bueno, I. Robles, Competitive adsorption of anionic and cationic molecules on three activated carbons derived from agroindustrial waste, Biomass-.-. Bioenergy 168 (2023) 106660, https://doi.org/10.1016/j.biombioe.2022.106660.

[33] E. Osorio, M.B. Ferraro, O.B. Oña, C. Cardenas, P. Fuentealba, W. Tiznado, Assembling small silicon clusters using criteria of maximum matching of the Fukui functions, J. Chem. Theory Comput. 7 (2011) 3995–4001, https://doi.org/10.1021/ct200643z.

[34] E.R. Johnson, S. Keinan, P. Mori-Sánchez, J. Contreras-García, A.J. Cohen, W. Yang, Revealing noncovalent interactions, J. Am. Chem. Soc. 132 (2010) 6498–6506, https://doi.org/10.1021/ja100936w.

[35] M. Gabriela Villamizar-Sarmiento, O. Yáñez, M.E. Flores, G. Álvarez-Acevedo, F. González-Nilo, J. Guerrero, I. Moreno-Villoslada, F.A. Oyarzun-Ampuero, Colloidal nanomedicines with prolonged release of chloroquine based on interactions with aromatic polymers after mixing two liquids: from in silico simulation of nanoparticle formation to efficient in-bench scale up, J. Mol. Liq. 395 (2024) 123906, https://doi.org/10.1016/j.molliq.2023.123906.

[36] C. Bannwarth, S. Ehlert, S. Grimme, GFN2-xTB—an accurate and broadly parametrized self-consistent tight-binding quantum chemical method with multipole electrostatics and density-dependent dispersion contributions, J. Chem. Theory Comput. 15 (2019) 1652–1671, https://doi.org/10.1021/acs.jctc.8b01176.

[37] P. Csizmadia, MarvinSketch and MarvinView: Molecule Applets for the World Wide Web, in: 1999.

[38] Marvin 23.5, Marvin was used for drawing, displaying, and characterizing chemical structures, substructures, and reactions, (2023).

[39] A. Dutta, P. Mondal, Density FUnctional Approach toward the Adsorption of Molecular Hydrogen as Well as the Formation of Metal Hydride on Bare and Activated Carbon-supported Rhodium Clusters, J. Phys. Chem. C. 122 (2018) 16925–16939, https://doi.org/10.1021/acs.jpcc.8b03142.

[40] X. Liu, Y. Han, Y. Cheng, G. Xu, Microwave-assisted ammonia modification of activated carbon for effective removal of phenol from wastewater: DFT and experiment study, Appl. Surf. Sci. 518 (2020) 146258, https://doi.org/10.1016/j.apsusc.2020.146258.

[41] Y. Zhao, N.E. Schultz, D.G. Truhlar, Design of density functionals by combining the method of constraint satisfaction with parametrization for thermochemistry, thermochemical kinetics, and noncovalent interactions, J. Chem. Theory Comput. 2 (2006) 364–382, https://doi.org/10.1021/ct0502763.

[42] S. Grimme, S. Ehrlich, L. Goerigk, Effect of the damping function in dispersion corrected density functional theory, J. Comput. Chem. 32 (2011) 1456–1465, https://doi.org/10.1002/jcc.21759.

[43] Y. Zhao, D.G. Truhlar, Exploring the limit of accuracy of the global hybrid meta density functional for main-group thermochemistry, kinetics, and noncovalent interactions, J. Chem. Theory Comput. 4 (2008) 1849–1868, https://doi.org/10.1021/ct800246v.

[44] R. Pino-Rios, O. Yañez, D. Inostroza, L. Ruiz, C. Cardenas, P. Fuentealba, W. Tiznado, Proposal of a simple and effective local reactivity descriptor through a topological analysis of an orbital-weighted fukui function, J. Comput. Chem. 38 (2017) 481–488, https://doi.org/10.1002/jcc.24699.
[45] R. Pino-Rios, O. Yañez, D. Inostroza, R. Báez-Grez, C. Cárdenas, W. Tiznado, Structure prediction using reactivity descriptors, in: S. Kaya, L. von Szentpály, G. Serdaroğlu, L. Guo (Eds.), Chemical Reactivity, Elsevier, 2023, pp. 449–462, https://doi.org/10.1016/B978-0-32-390259-5.00023-8.
[46] O. Yañez, R. Báez-Grez, D. Inostroza, R. Pino-Rios, W.A. Rabanal-León, J. Contreras-García, C. Cardenas, W. Tiznado, Kick–Fukui: a Fukui function-guided method for molecular structure prediction, J. Chem. Inf. Model 61 (2021) 3955–3963, https://doi.org/10.1021/acs.jcim.1c00605.
[47] G.F. Metha, M.A. Addicoat, Kick: constraining a stochastic search procedure with molecullar fragments, J. Comput. Chem. 30 (2009) 57–64, https://doi.org/10.1002/jcc.21026.
[48] P. Fuentealba, E. Florez, W. Tiznado, Topological analysis of the fukui function, J. Chem. Theory Comput. 6 (2010) 1470–1478, https://doi.org/10.1021/ct100022w.
[49] O. Yañez, A. Vásquez-Espinal, D. Inostroza, L. Ruiz, R. Pino-Rios, W. Tiznado, A Fukui function-guided genetic algorithm. Assessment on structural prediction of Sin (n = 12–20) clusters, J. Comput. Chem. 38 (2017) 1668–1677, https://doi.org/10.1002/jcc.24810.
[50] W. Tiznado, E. Chamorro, R. Contreras, P. Fuentealba, Comparison among four different ways to condense the Fukui function, J. Phys. Chem. A 109 (2005) 3220–3224, https://doi.org/10.1021/jp0450787.
[51] P. Fuentealba, P. Pérez, R. Contreras, On the condensed Fukui function, J. Chem. Phys. 113 (2000) 2544–2551.
[52] P. Fuentealba, H. Preuss, H. Stoll, L. Von Szentpály, A proper account of core-polarization with pseudopotentials: single valence-electron alkali compounds, Chem. Phys. Lett. 89 (1982) 418–422, https://doi.org/10.1016/0009-2614(82)80012-2.
[53] P. Fuentealba, L. Von Szentpaly, H. Preuss, H. Stoll, Pseudopotential calculations for alkaline-earth atoms, J. Phys. B: At. Mol. Phys. 18 (1985) 1287.
[54] W. Küchle, M. Dolg, H. Stoll, H. Preuss, Ab initio pseudopotentials for Hg through Rn: I. Parameter sets and atomic calculations, Mol. Phys. 74 (1991) 1245–1263.
[55] A. Bergner, M. Dolg, W. Küchle, H. Stoll, H. Preuß, Ab initio energy-adjusted pseudopotentials for elements of groups 13–17, Mol. Phys. 80 (1993) 1431–1441.
[56] M.J. Frisch, G.W. Trucks, H.B. Schlegel, G.E. Scuseria, M.A. Robb, J.R. Cheeseman, G. Scalmani, V. Barone, B. Mennucci, G.A. Petersson, H. Nakatsuji, M. Caricato, X. Li, H.P. Hratchian, A.F. Izmaylov, J. Bloino, G. Zheng, J.L. Sonnenberg, M. Hada, M. Ehara, K. Toyota, R. Fukuda, J. Hasegawa, M. Ishida, T. Nakajima, Y. Honda, O. Kitao, H. Nakai, T. Vreven, J.A. Montgomery, J.E. Peralta, F. Ogliaro, M. Bearpark, J.J. Heyd, E. Brothers, K.N. Kudin, V.N. Staroverov, R. Kobayashi, J. Normand, K. Raghavachari, A. Rendell, J.C. Burant, S.S. Iyengar, J. Tomasi, M. Cossi, N. Rega, J. M. Millam, M. Klene, J.E. Knox, J.B. Cross, V. Bakken, C. Adamo, J. Jaramillo, R. Gomperts, R.E. Stratmann, O. Yazyev, A.J. Austin, R. Cammi, C. Pomelli, J.W. Ochterski, R.L. Martin, K. Morokuma, V.G. Zakrzewski, G.A. Voth, P. Salvador, J.J. Dannenberg, S. Dapprich, A.D. Daniels, Farkas, J.B. Foresman, J.V. Ortiz, J. Cioslowski, D.J. Fox, Gaussian 09, Revision C.01, Gaussian 09, Revision C.01, Gaussian, Inc., Wallingford CT (2010).
[57] L. Goerigk, S. Grimme, A thorough benchmark of density functional methods for general main group thermochemistry, kinetics, and noncovalent interactions, Phys. Chem. Chem. Phys. 13 (2011) 6670–6688, https://doi.org/10.1039/c0cp02984j.
[58] T. Ziegler, A. Rauk, On the calculation of bonding energies by the Hartree Fock Slater method, Theor. Chim. Acta 46 (1977) 1–10, https://doi.org/10.1007/BF02401406.
[59] K. Kitaura, K. Morokuma, A new energy decomposition scheme for molecular interactions within the Hartree-Fock approximation, Int J. Quantum Chem. 10 (1976) 325–340, https://doi.org/10.1002/qua.560100211.
[60] E.J. Baerends, T. Ziegler, J. Autschbach, D. Bashford, A. Bérces, F.M. Bickelhaupt, C. Bo, P.M. Boerrigter, L. Cavallo, D.P. Chong, others, ADF2017, SCM, Theoretical Chemistry, Vrije Universiteit, Amsterdam, The Netherlands, ADF. Available Online: Http://Www. Scm. Com (Accessed on 20 April 2020) (2014).
[61] M.P. Mitoraj, Bonding in ammonia borane: an analysis based on the natural orbitals for chemical valence and the extended transition state method (ETS-NOCV), J. Phys. Chem. A 115 (2011) 14708–14716, https://doi.org/10.1021/jp209712s.
[62] S. Grimme, J. Antony, S. Ehrlich, H. Krieg, A consistent and accurate ab initio parametrization of density functional dispersion correction (DFT-D) for the 94 elements H-Pu, J. Chem. Phys. 132 (2010) 154104, https://doi.org/10.1063/1.3382344.
[63] S.F. Boys, F. Bernardi, The calculation of small molecular interactions by the differences of separate total energies. Some procedures with reduced errors, Mol. Phys. 19 (1970) 553–566, https://doi.org/10.1080/00268977000101561.
[64] J. Contreras-García, E.R. Johnson, S. Keinan, R. Chaudret, J.P. Piquemal, D. N. Beratan, W. Yang, NCIPLOT: a program for plotting noncovalent interaction regions, J. Chem. Theory Comput. 7 (2011) 625–632, https://doi.org/10.1021/ct100641a.
[65] T. Lu, Q. Chen, Independent gradient model based on Hirshfeld partition: a new method for visual study of interactions in chemical systems, J. Comput. Chem. 43 (2022) 539–555, https://doi.org/10.1002/jcc.26812.
[66] T. Lu, F. Chen, Multiwfn: a multifunctional wavefunction analyzer, J. Comput. Chem. 33 (2012) 580–592, https://doi.org/10.1002/jcc.22885.
[67] A.E. Reed, R.B. Weinstock, F. Weinhold, Natural population analysis, J. Chem. Phys. 83 (1985) 735–746.
[68] F. Weinhold, Natural bond orbital analysis: a critical overview of relationships to alternative bonding perspectives, J. Comput. Chem. 33 (2012) 2363–2379.
[69] E.D. Glendening, J.K. Badenhoop, A.E. Reed, J.E. Carpenter, J.A. Bohmann, C.M. Morales, C.R. Landis, F. Weinhold, Natural bond orbital analysis program: NBO 6.0, Theoretical Chemistry Institute, University of Wisconsin, Madison, WI (2013).
[70] W. Humphrey, A. Dalke, K. Schulten, VMD: visual molecular dynamics, J. Mol. Graph 14 (1996) 33–38, https://doi.org/10.1016/0263-7855(96)00018-5.
[71] C. Bannwarth, S. Ehlert, S. Grimme, GFN2-xTB—an accurate and broadly parametrized self-consistent tight-binding quantum chemical method with multipole electrostatics and density-dependent dispersion contributions, J. Chem. Theory Comput. 15 (2019) 1652–1671, https://doi.org/10.1021/acs.jctc.8b01176.
[72] S. Grimme, C. Bannwarth, P. Shushkov, A robust and accurate tight-binding quantum chemical method for structures, vibrational frequencies, and noncovalent interactions of large molecular systems parametrized for all spd-block elements (Z = 1–86), J. Chem. Theory Comput. 13 (2017) 1989–2009, https://doi.org/10.1021/acs.jctc.7b00118.
[73] J.-P. Ryckaert, G. Ciccotti, H.J.C. Berendsen, Numerical integration of the cartesian equations of motion of a system with constraints: molecular dynamics of n-alkanes, J. Comput. Phys. 23 (1977) 327–341, https://doi.org/10.1016/0021-9991(77)90098-5.
[74] V. Bernal, L. Giraldo, J.C. Moreno-Piraján, Adsorption of pharmaceutical aromatic pollutants on heat-treated activated carbons: effect of carbonaceous structure and the adsorbent–adsorbate interactions, ACS Omega 5 (2020) 15247–15256, https://doi.org/10.1021/acsomega.0c01288.
[75] M.P. Mitoraj, A. Michalak, Theoretical description of halogen bonding – an insight based on the natural orbitals for chemical valence combined with the extended-transition-state method (ETS-NOCV), J. Mol. Model 19 (2013) 4681–4688, https://doi.org/10.1007/s00894-012-1474-4.
[76] H. Kaur, A. Bansiwal, G. Hippargi, G.R. Pophali, Effect of hydrophobicity of pharmaceuticals and personal care products for adsorption on activated carbon: adsorption isotherms, kinetics and mechanism, Environ. Sci. Pollut. Res. 25 (2018) 20473–20485, https://doi.org/10.1007/s11356-017-0054-7.
[77] Z. Chen, Y. Zhang, M. Zhou, K. Yin, Y. Zhou, P. Cui, Z. Zhu, L. Zhong, Y. Wang, Mechanism analysis and process optimization of acetone–methanol azeotrope separation using 1-ethyl-3-methylimidazolium acetate based mixed extractants, J. Clean. Prod. 379 (2022) 134687, https://doi.org/10.1016/j.jclepro.2022.134687.
[78] S. Cao, R. Zhu, D. Wu, H. Su, Z. Liu, Z. Chen, How hydrogen bonding and π–π interactions synergistically facilitate mephedrone adsorption by bio-sorbent: an in-depth microscopic scale interpretation, Environ. Pollut. 342 (2024) 123044, https://doi.org/10.1016/j.envpol.2023.123044.
[79] Y. Zhang, S. Zhang, S. Xu, F. Cao, X. Ren, Q. Sun, L. Yang, R. Wennersten, N. Mei, Simulation of the VOC adsorption mechanism on activated carbon surface by nitrogen-containing functional groups, Appl. Sci. 14 (2024) 1793, https://doi.org/10.3390/app14051793.
[80] W. Xiao, D. Wang, Z. Shen, S. Li, H. Li, Multi-body interactions in molecular docking program devised with key water molecules in protein binding sites, Molecules 23 (2018), https://doi.org/10.3390/molecules23092321.